

U.S. Department of Commerce
National Oceanic and Atmospheric Administration
National Weather Service
National Centers for Environmental Predictions
5830 University Research Court
College Park, MD 20740

NCEP Office Note 507
<https://doi.org/10.25923/rb1n-za92>

**Direct Radiative Effects of Aerosols on Numerical Weather Forecast
-- A Comparison of Two Aerosol Datasets in the NCEP GFS**

Anning Cheng¹, and Fanglin Yang²
¹. IMSG@NCEP/EMC, ². EMC/NCEP, NOAA,

Abstract

This study compares aerosol direct radiative effects on numerical weather forecasts made by the NCEP Global Forecast Systems (GFS) with two different aerosol datasets, the OPAC and MERRA2 aerosol climatologies. The OPAC overestimates the aerosol loading from sea salt in storm track regions over the Northern and Southern Hemisphere ocean and underestimates the aerosol loading over most continents. The experiments made with MERRA2 aerosols showed improvements in GFS forecasts of aerosol optical depth (AOD) over the globe when verified against satellite retrievals. The experiment made with the OPAC aerosols largely underestimated the AOD over northwest Africa, central to east Africa, southeast Asia, and the Indo-Gangetic Plain, and overestimated the AOD in the storm track regions in both hemispheres. Surface downward short-wave (SW) and long-wave (LW) fluxes and the top of the atmosphere SW and outgoing LW fluxes from model forecasts are compared with CERES satellite observations. Forecasts made with OPAC aerosols have large AOD biases, especially in northwest Africa and the storm track regions. These biases are reduced in the forecasts made with MERRA2 aerosols. The improvements are most noticeable in the surface downward SW fluxes. GFS medium-range weather forecasts made with the MERRA2 aerosols demonstrated improved forecast accuracy of circulation and precipitation over the India and East Asian summer monsoon region. Forecasts of Africa easterly jets are also improved. Impacts on large-scale skill scores such as 500hPa geopotential height anomaly correlation are generally positive in the Northern Hemisphere and the Pacific and North American regions in the winter and summer seasons.

1. Introduction

Aerosols play an important role in the energy budget of the Earth-Atmosphere system. They directly scatter and absorb electromagnetic radiation (aerosol direct effects, e.g., Twomey, 1977), while indirectly interacting with cloud macro- and micro-physics, to such an extent that it changes the lifetime of clouds (aerosol indirect effect, e.g., Lohmann and Feichter, 2005; Quaas and Boucher, 2011). The non-absorbing aerosols such as sulfate and organic carbon scatter solar radiation back to space and produce a cooling effect on the climate system. Aerosols also contain absorbing material such as black carbon, which absorbs solar radiation and produces a warming effect to partly offset the aerosol cooling effect.

Aerosols and clouds continue to contribute the largest uncertainty to the energy budget of the earth system according to the IPCC Fifth Assessment Report (AR5, Boucher et al. 2013). Aerosol direct radiative forcing retrieved from satellite and ground measurements supplemented by global chemical transport simulations showed a cooling effect on the Earth-Atmosphere system. The effective radiative forcing (ERF) from aerosol-radiation interactions (direct effect) is assessed to be -0.45 K, with an uncertainty ranging from -0.95K to 0.05K (IPCC AR5, Boucher et al. 2013). Because of the uncertainties in sources and sinks of both natural and anthropogenic aerosols, the ERF from aerosol and climate feedback is $\pm 0.2 \text{ Wm}^{-2}\text{K}^{-1}$, with low confidence from a limited number of modeling studies (IPCC AR5, Boucher et al. 2013).

Currently there are four different approaches of varying complexity to incorporate aerosol effects into climate and numerical weather prediction (NWP) models. The first approach is to use monthly mean aerosol climatologies with a single-moment microphysics. Only aerosol direct effects are considered in this approach. The climatological aerosols used in this approach are the Optical Properties of Aerosols and Clouds (OPAC, Hess et al. 1998) used by the United States National Weather Service (NWS) Global Forecast System (GFS) for the past twenty years, and the Copernicus Atmosphere Monitoring System (CAMS, Bozzo et al. 2017) aerosols used by the ECMWF Integrated Forecasting System (IFS). The second approach is to use the monthly mean climatological aerosols with a double-moment microphysics. Both direct- and indirect- effects are included. This approach bears an additional computational cost because of the advections of one or more traces and more sophisticated physical processes depending on the schemes used. The third approach is to use a chemistry model with a single-moment microphysics. The nonhomogeneity of aerosols in space and time is well represented. Only aerosol direct effects on the forecast of meteorological fields are considered in this approach. The most advanced approach is to couple an aerosol-chemistry-transport model with a meteorological forecast model that employs a double moment microphysics scheme, and takes both the direct and indirect aerosol effects into consideration. Many General Circulation Models (GCMs) that participated in the IPCC

Report adopted this approach because GCMs are usually run at a rather coarse resolution, and are thus computationally less expensive than NWP models. Unlike GCMs, NWP models also need to make real-time forecasts and deliver products for forecasters within a limited time period.

It is worth noting that the level of sophistication used in climate models to represent various aerosol processes varies because our understanding of aerosol, cloud, and radiation interactions is still limited.

The same variation also exists among NWP models in the weather forecast community. Weather forecast skill does not always improve in NWP models that employ more sophisticated aerosol-cloud-radiation interaction schemes. Additional computational cost is also a major concern for NWP applications. From the experiments made with the GEOS-5 (Goddard Earth Observing System) atmospheric model coupled with the GOCART aerosol model, Reale et al. (2011) found that the global mean 500 hPa geopotential height anomaly correlations were not improved despite the fact that at the local scale significant aerosol events such as large wildfires and dust outbreaks were well simulated. Mulcahy et al. (2014) investigated the impact of aerosol complexity represented by the Met Office NWP model on its forecast skill. They found that the influence of indirect aerosol effects on the large-scale circulation and global precipitation pattern are generally small for short and medium range forecasts. However, including the indirect effects can result in strengthening the low-level monsoon flow and causing heavier precipitation over Southeast Asia, which compared well with observations.

In addition to climate and NWP models, a Single Column Model (SCM) is extensively used for an idealized case study with highly simplified assumptions for aerosols. An SCM is much more computationally affordable and allows for easy testing of a wide variety of model modifications. Many case studies were organized by the Global Energy and Water Experiment Cloud System Study (GCSS) Boundary Layer Cloud Working Group and later by the Global Atmosphere System Studies (GASS) Panel. For example, the number concentration of liquid drops and ice crystals representing effects of aerosols are treated as a constant in the Dynamics and Chemistry of Stratocumulus II (DYCOMS-II) experiments (Ackerman et al. 2009). Lebassi-Habtezion and Caldwell (2015) compared different aerosol specifications in the SCM mode of version 5 of the Community Atmosphere Model (SCAM5) on the low biases of aerosols, cloud droplets, and ice crystal concentrations. However, there is no SCM study on direct and indirect aerosol effects as far as we know.

It is also known that even for aerosol direct radiative effects large uncertainties exist in the computation of aerosol optical properties. These uncertainties can affect the accuracy of aerosol radiative forcing and subsequently weather and climate model forecast skill. By applying a monthly varying aerosol climatology rather than a fixed climatology in the ECMWF IFS, Rodwell and Jung (2008) reported an improvement in forecast skill at

5 to 10-day lead times in the tropics and extratropics. Bozzo et al. (2017) replaced the aerosol climatology in ECMWF IFS with CAMS for the period 2003-2014. They found that the impact of CAMS aerosols on conventional forecast skill scores and large-scale weather patterns was small; however, significant local aerosol impacts on summer monsoon circulations were noticed over the northern Indian Ocean and the Arabian peninsula.

In this study, we first compare the OPAC aerosol climatology, which has been used by the GFS for more than 20 years, with the relatively new MERRA2 (Modern-Era Retrospective analysis for Research and Applications, Version 2) aerosol climatology. Then we will carry out numerical simulations to assess the impact of MERRA2 on GFS forecast skill. The main goal of this study is to further our understanding of the direct effects on the radiation budget, global and local circulation patterns, and the predictive skill of a high quality dataset in a high-resolution operational NWP model.

The rest of the paper is organized as follows. Section 1.2 briefly describes the source of the aerosol datasets. Section 2 introduces the experiment design. Results are presented in Section 3. A summary and conclusions are given in Section 4.

1.2. Aerosol Climatologies

OPAC provides microphysical and optical properties for ten aerosol components. The extinction, scattering, and absorption coefficients, the single scattering albedo, the asymmetry parameter, and the phase function are calculated assuming spherical particles for aerosols. Data for sixty one wavelengths between 0.25 μm and 40 μm and eight values of the relative humidity are given. The real aerosol in the atmosphere can be a mixture of the basic components. The vertical structure of the aerosol is calculated on the basis of exponential aerosol height profiles. OPAC aerosol used by the GFS over the past twenty years has a horizontal grid-spacing of approximately 5 degrees based upon observations made before 1998 (Table 1).

MERRA2 was made with the Modern-Era Retrospective analysis for Research and Applications Version 2 (Buchard et al, 2017; Randles et al, 2017) which used the three-dimensional variational data analysis (3DVAR) Gridpoint Statistical Interpolation (GSI) meteorological analysis scheme and GEOS-5 atmospheric model. The MERRA-2 meteorological observing system includes the Moderate Resolution Imaging Spectroradiometer (MODIS) and Advanced Very High Resolution Radiometer (AVHRR) instruments, the Multi Angle Imaging SpectroRadiometer (MISR) and ground-based Aerosol Robotic Network (AERONET), and other numerous additions and bias-corrected systems.

Table 1. OPAC and MERRA2 aerosol climatology comparison

	OPAC	MERRA2
Horizontal resolution	5 by 5 degree	0.5 by 0.625 degree
Vertical levels	5 regimes (One layer/two layers)	72 (Surface to 1 Pa)
Aerosol types	10 (1 insoluble, 1 soluble, 2 sea salt, 4 mineral, 1 soot, 1 sulfate)	15 (5 dust, 5 sea salt, 2 organic carbon, 2 black carbon, 1 sulfate)
Stratosphere volcano	Background (1.e-4)	Assimilated sea salt and sulfate
Data Collected	Before 1998	2003-.

One of the reasons for us to replace OPAC with MERRA2 is to take advantage of the higher spatial resolution MERRA2 offers (Table 1). The horizontal resolution of OPAC is 5 degrees by 5 degrees. In the vertical, OPAC aerosols have one layer near the surface, whose concentration is assumed to exponentially decrease to the model top. MERRA2 has a horizontal grid-size of 0.5 degrees by 0.625 degrees and 72 vertical levels ranging from surface to 1 Pa. In addition, MERRA2 has 15 modes instead of the 10 modes in OPAC and assimilates volcanoes in the stratosphere, while OPAC contains a constant background of volcanic aerosols.

2. Experimental Design

The GFS version 16 (GFS.v16) (Yang et al, 2020), which has a horizontal resolution of ~13 km and 127 levels in the vertical extending to the mesopause (C768L128 GFS), is used for this study. Data at certain specific locations extracted from the GFS are also used to drive the Common Community Physics Package (CCPP) Single Column Model (SCM). GFS.v16 was implemented into operations in March 2021. It uses the GFDL¹ microphysics (Zhou et al. 2019) and the Rapid Radiation Transfer Model for GCM (RRTMG, Mlawer et al., 1997; Mlawer and Clough, 1998; Mlawer, et al., 2016).

The GFDL microphysics, a single-moment scheme, advects and predicts the mixing ratios of condensates and hydrometers, but not their number concentrations. There is no explicit activation of ice nuclei (IN) or cloud condensation nuclei (CCN). The ice and liquid fractions of mixed-phase clouds are parameterized based on temperature only. Therefore, the aerosol indirect effect is not included in this study.

For radiation, a correlated-k distribution and a transmittance lookup table scaled by

¹ Geophysical Fluid Dynamics Laboratory

optical depth are used in RRTMG to achieve high efficiency and accuracy. 140 unevenly distributed g-points (quadrature points) in 16 broad spectral long wave (LW) bands and 112 g-points in 14 shortwave (SW) bands are included for the major atmospheric absorbing gasses of ozone, water vapor, carbon dioxide and various minor absorbing species such as methane, nitrous oxide, and oxygen. In order to represent the unresolved subgrid-scale cloud variability, a Monte-Carlo Independent Column Approximation (McICA) method is adapted in RRTMG. Look up tables (LUTs) for the extinction, scattering, single scattering albedo, and asymmetry factor are provided by MERRA2 for each solar spectral band, and for each relative humidity interval for hydrophilic aerosol. They are computed as (Hou et al. 2002):

$$\delta_v = \bar{N} \sum c_i \delta_{vi} \quad (1)$$

$$\omega_v = \sum c_i \omega_{vi} \delta_{vi} / \sum c_i \delta_{vi} \quad (2)$$

$$g_v = \sum c_i g_{vi} \sigma_{vi} / \sum c_i \sigma_{vi} \quad (3)$$

Where c_i is the mixing ratio of the i^{th} aerosol component, δ_{vi} , σ_{vi} , ω_{vi} , and g_{vi} are coefficients for extinction, scattering, single scattering albedo, and asymmetry factor, respectively, for a spectral band v . N is the climatological mean value of aerosol particle number density in the domain.

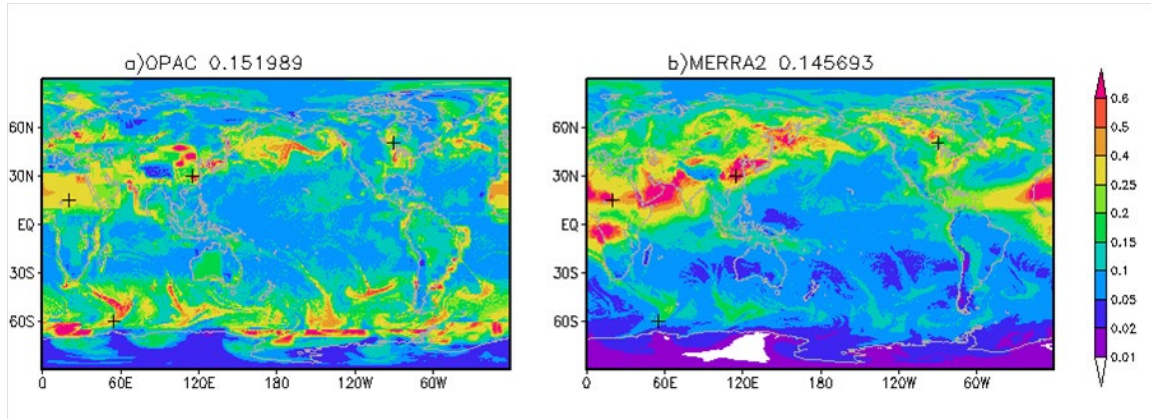


Figure 1. Global distribution of total aerosol optical depth (AOD) at 550 nm averaged for the first 24 hours of C768L127 GFS.v16 forecasts initialized at 2020/07/10 00UTC. The left panel shows the total AOD from the experiment using the OPAC aerosol climatology, and the right panel from the experiment using the MERRA2 aerosol climatology.

The CCPP_SCM with 127 levels, the same levels used by GFS.v16, is used to study the direct influence of aerosols on radiation fluxes. Initial conditions and forcing data are extracted from a GFS.v16 free forecast initialized at 00Z of July 10, 2020. Four clear-sky cases, at locations marked by four black crosses in Figure 1, are chosen for the Sahara Desert, Northeast CONUS, the Southern Ocean, and Southeast Asia, respectively, to perform the SCM experiments.

In order to assess the impact of replacing the OPAC with MERRA2 aerosols in the

GFS on local circulations and global forecast skill, two control experiments with OPAC aerosols and two sensitivity experiments with MERRA2 aerosols were conducted for one summer and one winter season, respectively. The winter case covers the period from 1 December 2019 through 1 March 2020, and the summer case covers the period from 1 June 2019 through 1 September 2019. Each experiment is initialized with GFS.v16 initial conditions at the 00Z cycle, once for every 5 days in each of the winter and summer seasons.

3. Results

3.1 Single Column Model Experiments

In order to exclude the influence of advection and complex interactions between aerosols and meteorological fields in the NWP model, the CCPP_SCM is first used to study the aerosol direct effect at a few selected sites in the Sahara Desert, Northeast Continental United States (CONUS), Southern Ocean, and Southeast Asia (black crosses in Figure 1). The CCPP_SCM has the same 127 levels as the GFS.v16. It is found that the total AOD in the Sahara Desert from the MERRA2 experiment is about two times larger than that from the OPAC experiment (Figure 2a). Dust makes the largest contribution to the total AOD (Figure 2b), followed by sulfate and organic carbon. Sulfate AOD from MERRA2 is much larger than that from OPAC, but the organic carbon AOD is slightly smaller (Figures 2c and d). Differences in the surface downward SW and LW between the two experiments are shown in Figure 2e. Larger AOD from aerosol loading causes less downward surface SW flux due to aerosol extinction. Aerosols also absorb incoming SW and LW fluxes emitted from the surface and the atmosphere itself, thus increasing atmospheric temperature in the aerosol layers. The differences in the surface downward SW flux between the two experiments are as large as 30 W/m^2 , while the differences in surface downward LW flux are about 5 W/m^2 . So the Beer-Lambert law dominates absorption and scattering. Larger aerosol loading from the MERRA2 experiment also leads to more SW reflection at the top of the atmosphere (TOA, Figure 2f). Although LW emissions are larger in layers where aerosol loadings are high, aerosols in these layers also absorb LW emissions from the earth surface and adjacent atmospheric layers. The net LW effect shows that the TOA outgoing LW radiation (OLR) flux from the MERRA2 experiment is about 0.3 W/m^2 smaller than that from the OPAC experiment. For the TOA aerosol, the aerosol net SW and LW effect is dominated by the reflection of SW fluxes. The MERRA2 case produces about 5 W/m^2 more energy loss at the TOA by the atmosphere than the OPAC case.

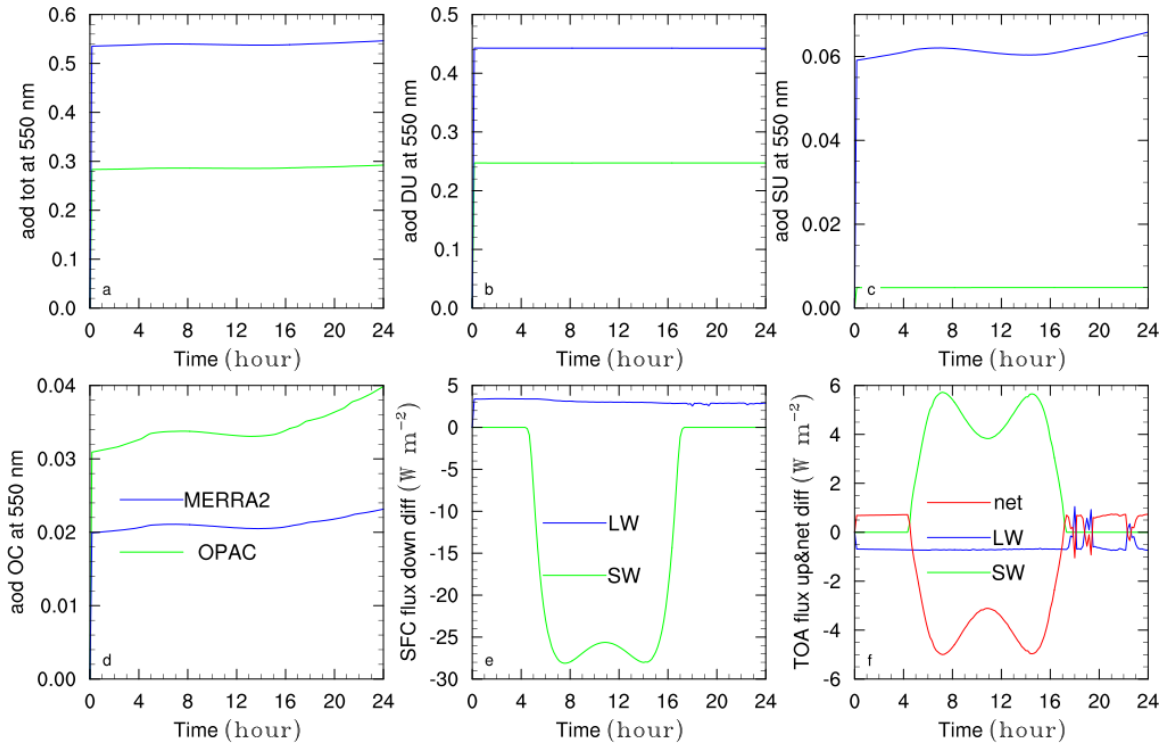


Figure 2. Time series of 24-hour forecasts in the Sahara desert for the total AOD (a), AOD of dust (b), AOD of sulfate (c), AOD of organic carbon (d), surface downward SW and LW fluxes (e), TOA upward SW, LW, and net fluxes (f), respectively. The AOD of black carbon and sea salt is much less than that of organic carbon, so not plotted.

Sulfate from industrial sources contributes the most to the aerosol AOD in Southeast Asia. Organic carbon is one order of magnitude less than sulfate, and black carbon about two orders less (Figures 3a-d). The AOD from sulfate is around 0.4 from MERRA2 (Figure 3b). It is important to note that the AOD from dust in the Sahara is also around 0.4 (Figure 2b). The absorption by sulfate is not as strong as by dust. The mean particle size of sulfate is 0.35 μm , while the mean particle size of dust ranges from 0.079 μm (bin 1) to 7.772 μm (bin 5). Particles with sizes close to or within the LW wavelength band have stronger absorption than other particles. This can be seen from the small difference in the surface downward LW flux between the OPAC and MERRA2 experiments (Figure 3e). Although the extinction of SW by sulfate is smaller than dust in surface downward SW comparisons, the reflection of SW at the TOA by sulfate is about two times greater than dust when comparing Figure 3f and Figure 2f.

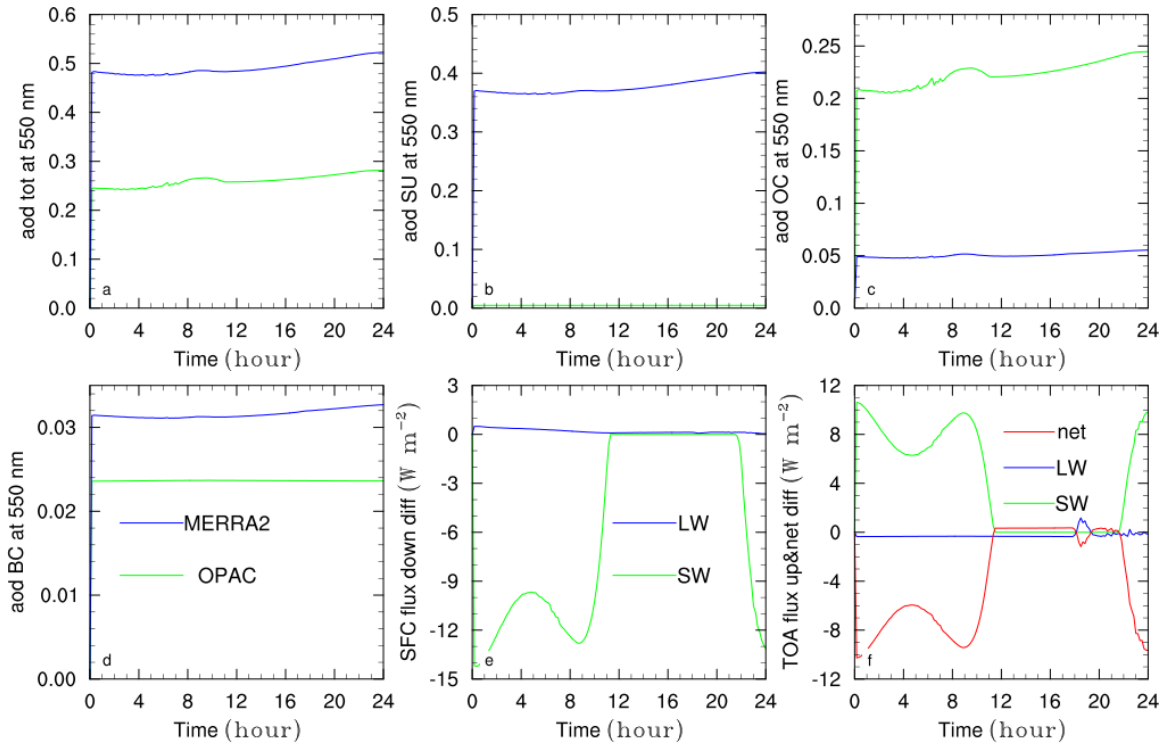


Figure 3. Same as Figure 2 except for Southeast Asia.

Organic carbon and sulfate contribute about the same to the total AOD in the MERRA2 experiment at the Northeast CONUS site. The contribution from dust is a few times less (Figures 4a-c). The OPAC experiment underestimates sulfate aerosol in both the Northeast CONUS and Southeast Asia regions, but overestimates organic carbon compared with the MERRA2 experiment. As in the previous experiments, the Beer-Lambert law dominates absorption and scattering. The difference in the surface downward SW flux between the two experiments using OPAC and MERRA2 is as large as $15 W/ m^{-2}$, while the difference of surface downward LW flux difference is about $2 W/m^{-2}$. It looks like the extinction and absorption of either organic carbon or sulfate is not as large as those of dust in the Sahara desert because the total AOD of both the CONUS and Sahara is about 0.5, but the surface downward shortwave and LW difference is two times less. The reflection of sulfate seems to be larger than that of dust because the TOA upward SW difference between the two experiments is as large as $11 W m^{-2}$, which is mainly contributed by sulfate from MERRA2, about twice the difference in the Sahara Desert.

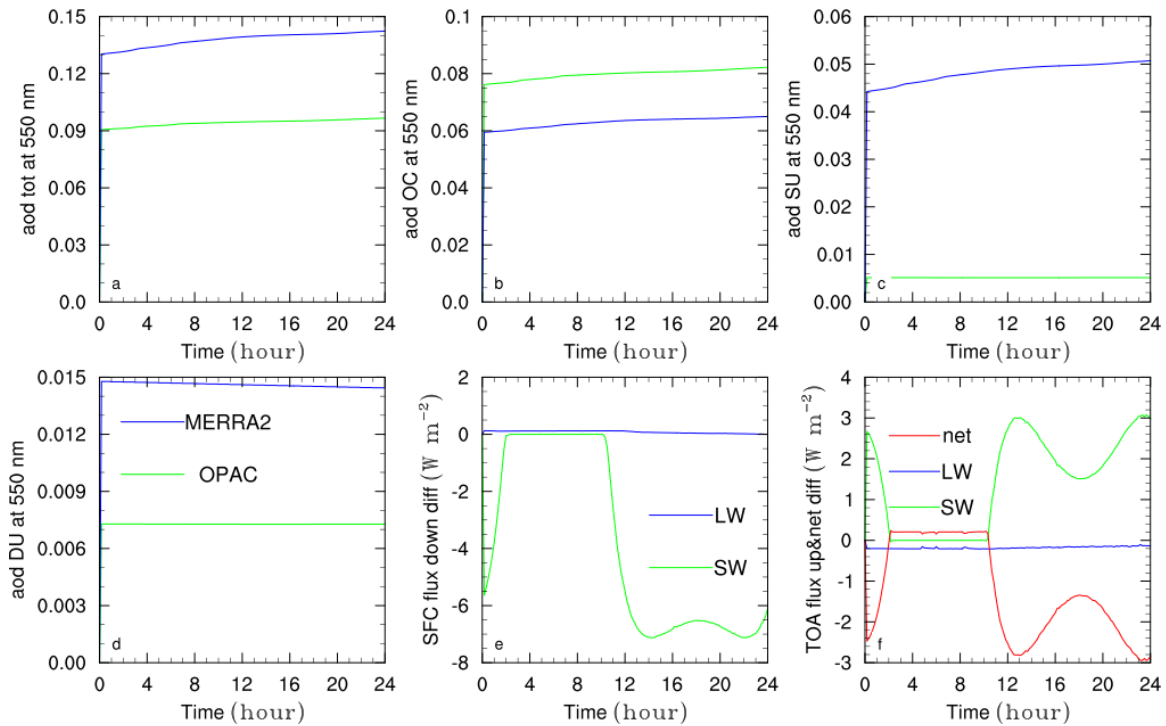


Figure 4. Same as Figure 3 except for Northeast CONUS.

Unlike at the other sites, OPAC AOD is larger than that of MERRA2 at the Southern Ocean site. This site is located in the Southern Hemisphere storm track region. Sea salt from sea spray is the major contributor to the total AOD. Organic carbon AOD and sulfate AOD are about one order of magnitude smaller than sea salt AOD (Figures 5a-d). However, LW absorption by sulfate is still the main reason for the positive surface LW between MERRA2 and OPAC. The absorbing aerosol loading of sea salt and organic carbon from MERRA2 is less than that from OPAC (Figures 5 b and c), and that of sulfate is more than that of the OPAC (Figure d). The greater sulfate loading is causing more absorption in the aerosol layer, resulting in more surface downward LW from MERRA2. The extinction effects and reflection of sea salt seems to be the smallest among all the SCM experiments, since the surface downward SW difference between the two experiments is less than 5 W m⁻² and TOA upward SW is less than 3 W m⁻².

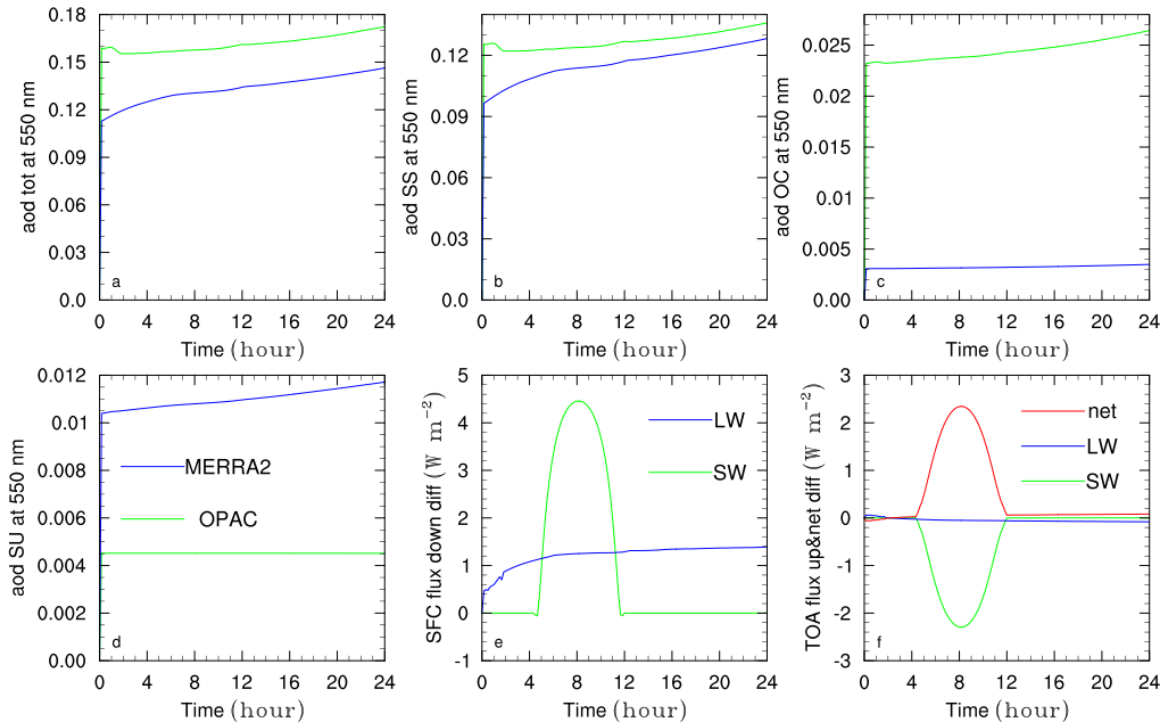


Figure 5. Same as Figure 4 except for the Southern Ocean.

In summary, total AOD is the major factor that determines the radiation fluxes. Differences in the surface downward SW flux between the two SCM experiments running with OPAC and MERRA2 aerosols is the largest, up to 30 W/m^2 , among all the radiative fluxes presented in this section. The difference of TOA upward SW flux ranks second, up to 10 W/m^2 . The differences in surface downward LW and TOA OLR are relatively small.

3.2 Global NWP Experiments

In this section, the differences in forecasted AOD and radiative fluxes from the GFSv16 experiments are evaluated. Shown in the top two panels of Figure 6 are global distributions of simulated AOD (550 nm) and downward SW flux at the surface for the experiment with OPAC aerosols at forecast T+120h (day 5) from the 2019 summer simulations. The middle panels show the AOD difference between MODIS retrievals and the OPAC experiment, and the difference in downward SW flux at the surface between CERES retrievals and the OPAC experiment, respectively. The differences in AOD and surface downward SW flux between the two experiments with OPAC and MERRA2 aerosols are presented in the bottom two panels. Large differences can be seen at different locations. The OPAC experiment has a much smaller AOD over Northwest Africa than the MERRA2 experiment because OPAC has less dust than MERRA2 in this region. The MERRA2 experiment agrees better with MODIS retrievals than the OPAC experiment. Dust originating in Africa is advected westward and lifted upward to the Atlantic Ocean and eastward to the Arabian Sea. Over central to eastern Africa, organic carbon from natural resources also contributes

to the simulated total AOD. The MERRA2 experiment also shows a better AOD distribution than the OPAC experiment in this region. Significantly higher AOD from the aerosol loading over Southeast Asia and over the Indo-Gangetic Plain can also be seen in the MERRA2 experiment and MODIS retrieval than in the OPAC experiment. As described in Section 3.1 for the SCM experiments, aerosols over Southeast Asia are mainly from anthropogenic sources due to industrialization. The aerosols that are responsible for the high AOD in Europe in the MERRA2 experiment have similar origins. Furthermore, the OPAC experiment has a widespread overestimation of AOD in the storm track regions in both the Southern and Northern Hemispheres. As described in Section 3.1, sea salt from sea sprays is the main source of aerosols in these regions.

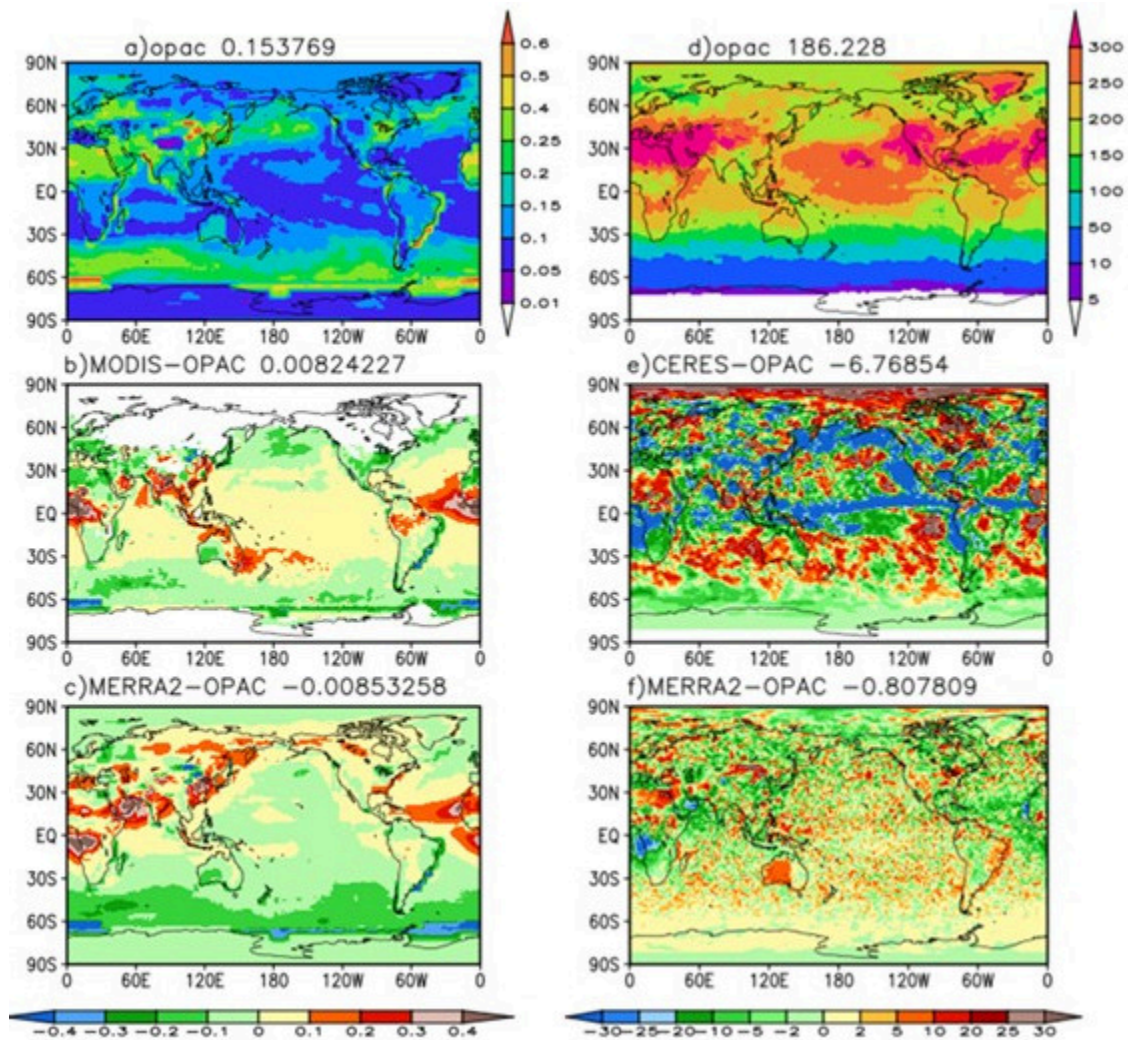


Figure 6. Global distributions of total AOD (a) and surface downward SW (d) at the T+120 forecast hour, averaged for the 2019 summer from the experiment with OPAC aerosols. The difference in AOD between MODIS retrievals and the experiment with OPAC aerosols is shown in (b), and the difference in surface downward SW between CERES and the experiment with OPAC aerosols in (e). The difference in AOD between the experiments

with MERRA2 and OPAC aerosols is shown in (c), and the corresponding difference of surface downward SW flux in (f). The numbers written at the top of each panel are the global averages.

Because of the extinction effect of aerosols, a larger AOD implies stronger reduction of downward SW flux at the surface. This can be seen in Figures 6e and 6f. The MERRA2 experiment shows larger reductions in surface downward SW fluxes than the OPAC experiment in Northwest Africa, Central to East Africa, Southeast Asia, and the Indo-Gangetic Plain but smaller reductions in the storm track regions of both hemispheres. The distributions are consistent with the differences of AOD shown in Figures 6b and 6c. The magnitudes of the SW differences shown in Figure 6 are in good agreement with those from the SCM experiments presented in Section 3.1. For example, the difference in the surface downward SW between the two experiments (Figure 6f) reached 30 W/m^2 along the west coast of North Africa and in the central-to-east Africa regions.

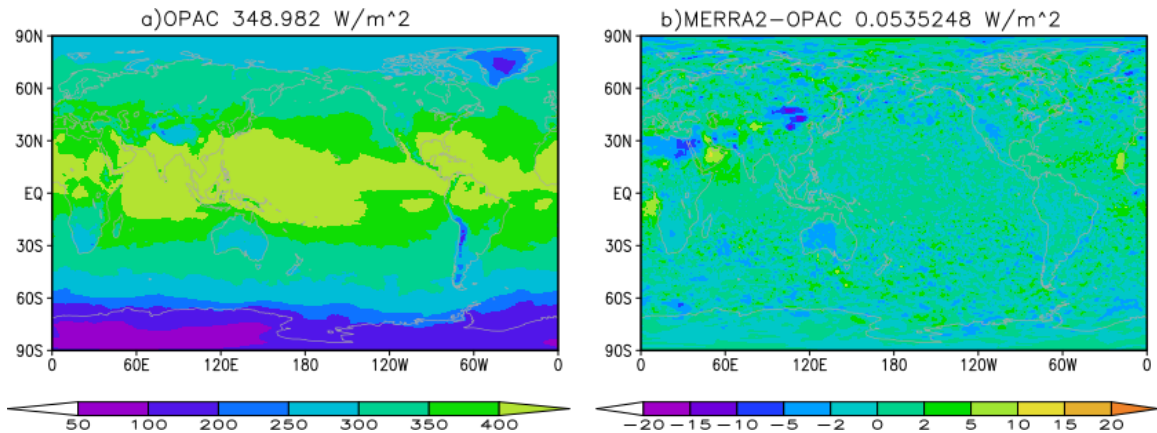


Figure 7. Global distribution of surface downward LW at T+120 hours averaged for the 2019 summer from the OPAC experiment (a), and the difference in surface downward LW between the MERRA2 and OPAC experiments in (b).

The absorption of LW radiation by aerosols has a warming effect on the atmosphere at aerosol layers. It increases atmospheric temperature at the aerosol layers and consequentially the downward LW fluxes at the surface. Compared to the OPAC experiment, the MERRA2 experiment shows a larger downward LW flux at the surface in regions where AOD is also larger (Figure 7). The magnitude of the difference is up to 10 W/m^2 in central-to-east Africa. As with the SCM studies, the strengths of absorption and emission of LW radiation by aerosols are proportional to the aerosol loading. The MERRA2 experiment shows a smaller TOA OLR in regions where AOD is larger (Figure 8). The AOD-OLR relationship is not as evident as shown in the downward SW and LW at the surface, likely due to the influence of clouds.

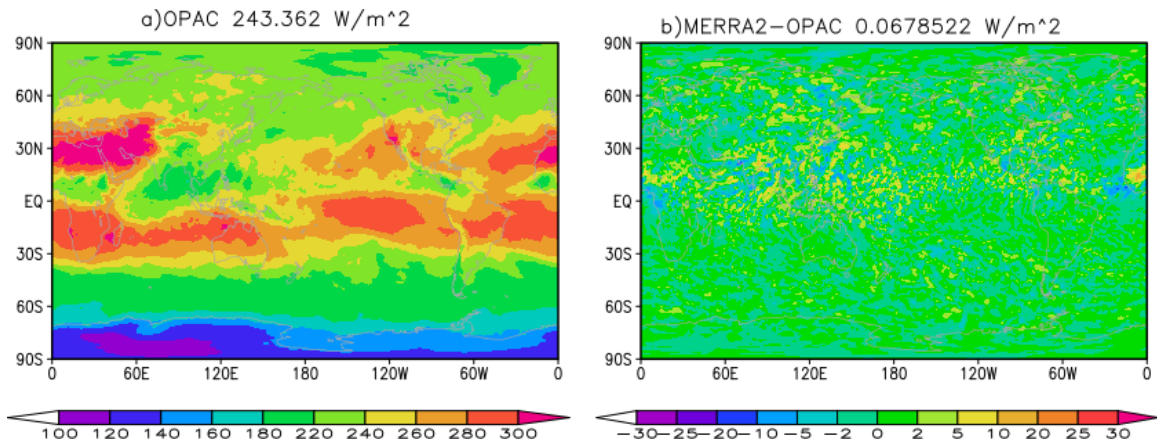


Figure 8. Same as Figure 7 except for OLR.

The reflection of SW is another important radiative forcing by aerosols (Figure 9). The difference is not as large as the surface downward SW, but relatively larger TOA reflected SW fluxes from the MERRA2 experiment can still be seen over Northwest Africa, central-to-east Africa, and Southeast Asia, and smaller TOA reflected SW in the Southern Hemisphere storm track region.

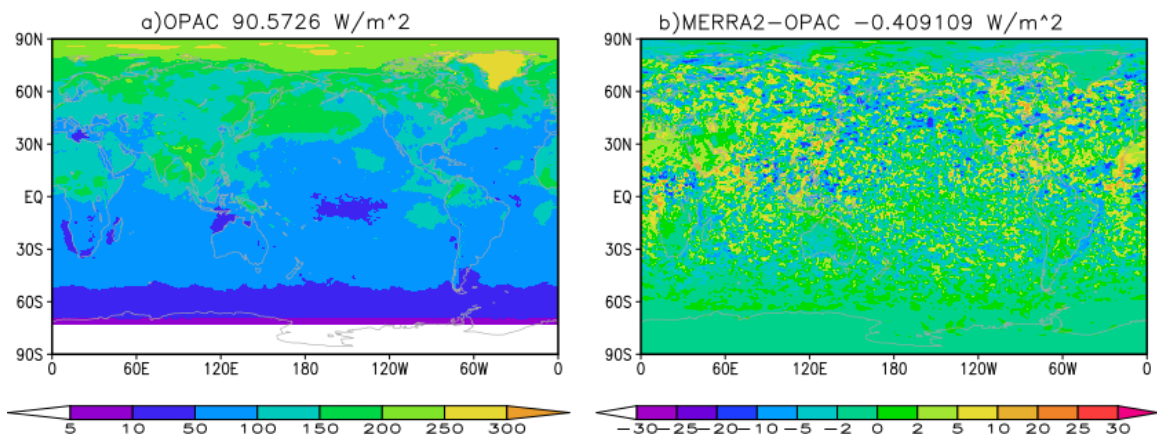


Figure 9. Same as Figure 8 except for TOA upward SW flux.

Overall, the radiative forcing by aerosols is highly inhomogeneous in both time and space. We will investigate the influence of aerosols on local circulation in the following sections.

3.2.1 Influence of Aerosols on Asian Monsoon

The distributions of simulated AOD at 550 nm and the surface downward SW flux in the Asian Monsoon region at T120h for the 2019 summer from the experiment with OPAC aerosols are shown in the top panels of Figure 10. The differences between satellite observations (MODIS for AOD and CERES for SW) and the OPAC experiment are shown in the middle panels, and the differences between the two experiments in the bottom panels.

AOD from the OPAC experiment is underestimated over the Arabian peninsula, Arabian Sea, and Indian subcontinent. These biases are reduced in the MERRA2 experiment which compares better with the MODIS retrievals (Figure 10b and Figure 10c). The reduced surface downward SW flux due to aerosol extinction is evident over the Arabian peninsula, but less clear over the Indian subcontinent, where monsoonal circulation and precipitation might have made the detection of aerosol direct radiative effects less obvious.

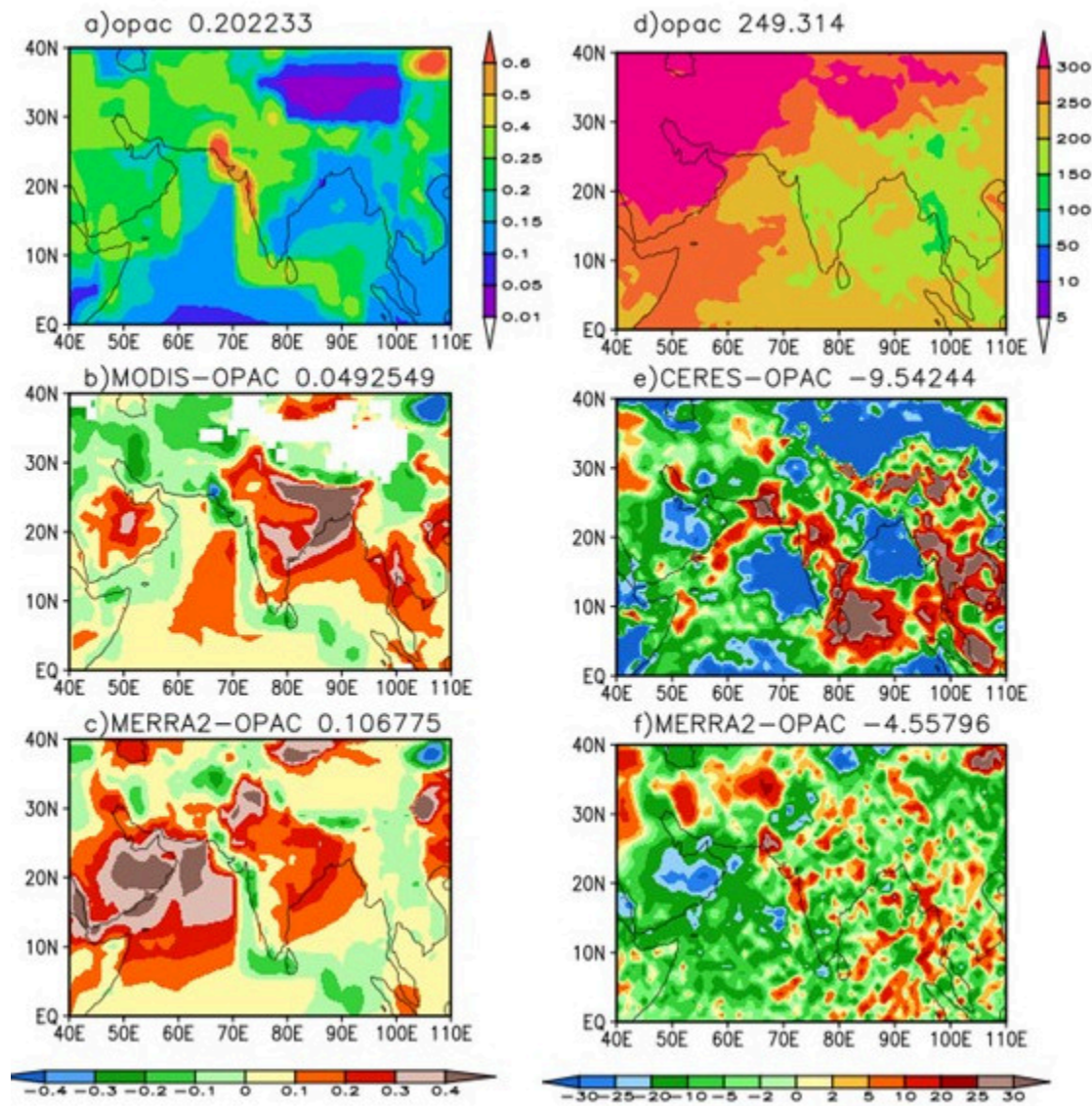


Figure 10. Same as Figure 6 except for Asian monsoon region.

Monsoon circulation as represented by the 850-hPa winds (Figure 11a) is well captured by the OPAC experiment. A surface low pressure system is found between 15°N and 35°N (Figure 11a). However, the OPAC experiment underestimates the surface pressure over the Arabian peninsula and overestimates the surface pressure over the Arabian Sea. This

results in an anomalous anticyclonic circulation over the Arabian peninsula (Figures 11b and 11c). The northward monsoonal flow over the Indian subcontinent is also stronger in the MERRA2 experiment, matching better with the NCEP reanalysis (denoted as OBS in the figures) than the OPAC experiment. The Monsoon is a complicated system and is affected by many different dynamical and physical processes. Aerosol radiative forcing does play a significant role in modulating monsoonal flow and precipitation in this region (e.g., Lau et al. 2008, Gautam et al. 2009, and Lee et al. 2014)

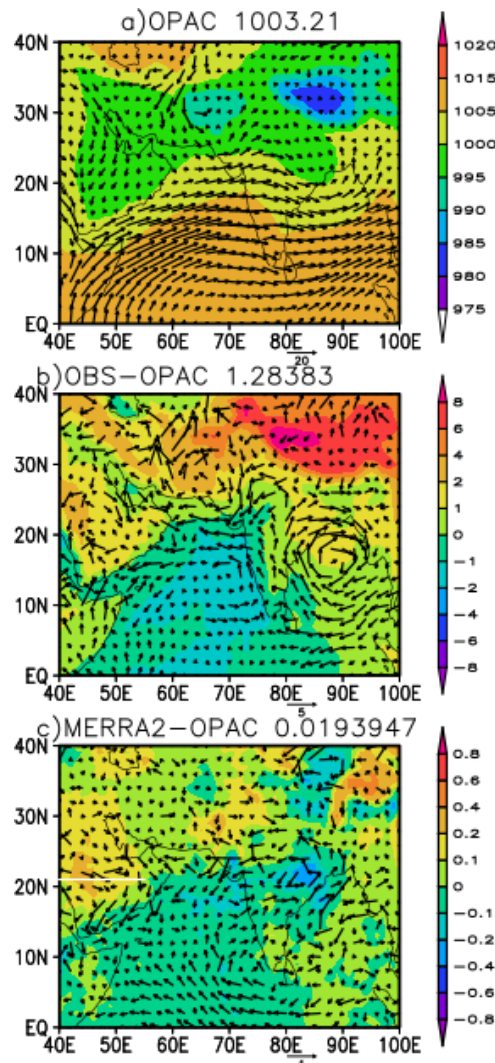


Figure 11. Distributions of sea level pressure (shaded) overlaid with 850-hPa vector winds at the T+120 hour averaged for the 2019 summer over the Asian monsoon region from the OPAC experiment in (a), difference between the NCEP reanalysis and the OPAC experiment in (b), and the difference between the MERRA2 and OPAC experiments in (c).

To better understand the impact of aerosols on the formation of monsoonal surface pressure systems, a vertical cross-sections of vertical velocity and temperature at 21°N covering longitudes from 40°E to 55°E is presented in Figure 12a for the OPAC experiment.

The differences between the MERRA2 and OPAC experiments and between the NCEP reanalysis and the OPAC experiment are shown in Figures 12b and 12c, respectively. Temperatures in Figure 12a decrease with height as expected. There is a slightly positive vertical velocity zone between 900 hPa and 600 hPa. The maps of temperature differences between the two experiments (Figure 12b) show a dipole pattern, e.g., cooling below 500 hPa and warming above. This pattern is also observed in the difference map between OPAC and the NCEP Reanalysis (Figure 12c). By comparing the aerosol number concentrations (Figure 12d), one can see that the dipole pattern is likely a reflection of aerosol direct radiative forcing in this region. The reflected SW can warm the atmosphere above and has a cooling effect on the aerosol layer. The emission of the LW also has similar effects. There are dominant downward motions embedded with small upward motions in both the MERRA2 experiment and NCEP reanalysis, which is typical for the high pressure regime. Because of the improved circulation in the MERRA2 experiment, surface precipitation from the MERRA2 experiment also compares better with the NCEP reanalysis than the OPAC experiment (Figure 13). Like in the NCEP reanalysis, precipitation from the MERRA2 experiment decreases over the Arabian peninsula and increases over the east Indian peninsula and Indian Ocean.

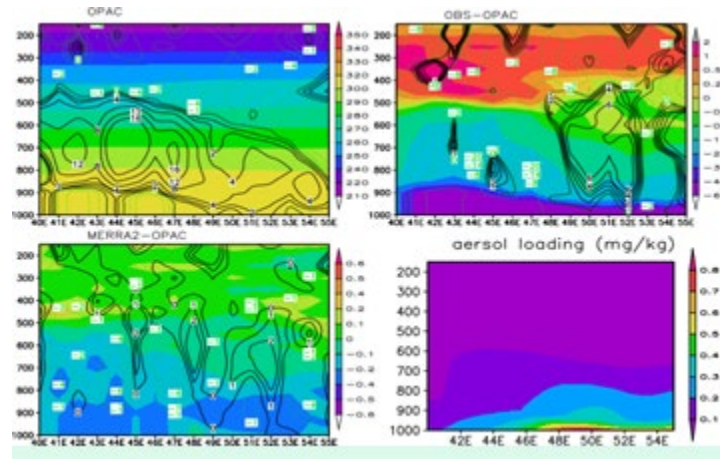


Figure 12. Zonal cross-sections of mean temperature overlaid with vertical velocity between 40°E and 100° E at 21°N at T+120 hours averaged over the 2019 summer over Asian monsoon region from the experiment with OPAC in (a, top-left panel). The differences between the NCEP reanalysis and OPAC experiment are shown in (b, top-right panel), and the differences between the MERRA2 and OPAC experiments (c, bottom-left panel), respectively. The aerosol loading for the same location and period is shown in the bottom-right panel (d).

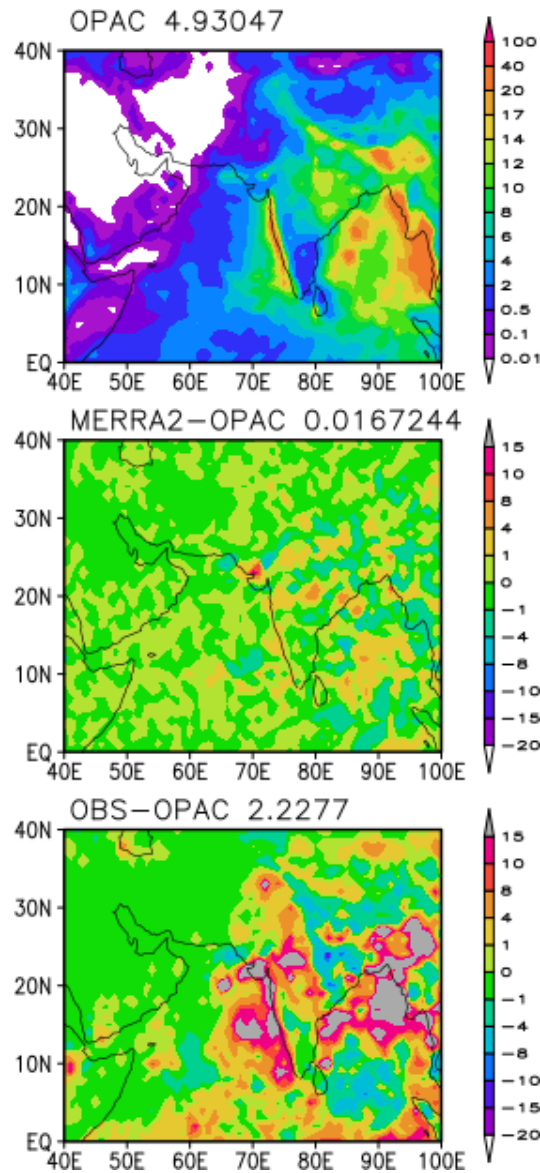


Figure 13. Surface precipitation over the Indian monsoon region at T+120 hours averaged for the 2019 summer from the OPAC experiment in (a), the difference between the NCEP reanalysis and OPAC experiment in (b), and the difference between the MERRA2 and OPAC experiments in (c).

3.2.2. Impact on African Easterly Jet

It is known that the African easterly jet (AEJ) plays an important role in the tropical easterly wave formation. Convective activities associated with these waves can trigger tropical storm genesis (Leroux, 2001). Figure 14a shows that the AEJ, as represented by the 600-hPa zonal wind at T+120 hours averaged for the 2019 summer over Northwest Africa from the OPAC experiment, is located between 10°N and 18°N and 30°W and 10°E. Compared with the NCEP reanalysis, the OPAC experiment underestimated the strength of the AEJ, but overestimated the easterlies north of the jet near 23°N and south of the jet

near 10°N (Figure 14b). The MERRA2 experiment produced a stronger AEJ and weaker easterlies on the north and south side of the jet (Figure 14c).

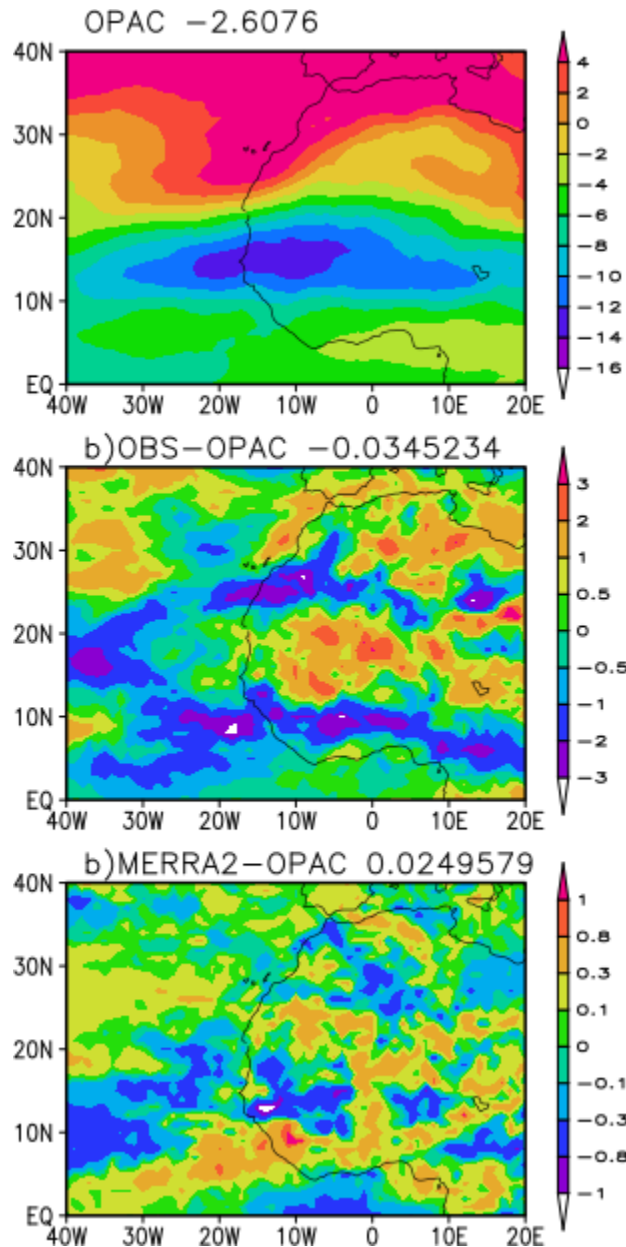


Figure 14. 600-hPa zonal wind at T+120 hours averaged for the 2019 summer over Northwest Africa from the OPAC experiment in (a), the difference between the NCEP reanalysis and the OPAC experiment in (b), and the difference between the MERRA2 and OPAC experiments in (c).

There is a low sea level pressure system in West Africa between 20°N and 35°N and 20°W and 20°E (Figure 15a). The low pressure system is weaker in the MERRA2 experiment, matching better with the NCEP Reanalysis (Figures 15 b and c). This low is associated with a stronger AEJ since high pressure corresponds to clockwise circulation

and easterly wind in the jet stream region. There is less aerosol loading from MODIS and the MERRA2 experiment in comparison with the OPAC experiment, and consequently more surface downward SW flux from both the CERES data and MERRA2 experiment (Figure 16). There is also less surface downward SW flux associated with more aerosol loading over the west coast of West Africa near 20°W and 15°N in the MERRA2 experiment and CERES observations than in the OPAC experiment. Regional impacts on the African Easterly Jet (AEJ) with the significant dust aerosols in the aerosol climatology has also been cited by Mulcahy et al. (2014). They found weakening on both the southern and northern flanks of the jet and a weakened jet from an enhanced low pressure from more aerosol loading in West Africa instead of less aerosol loading as found here.

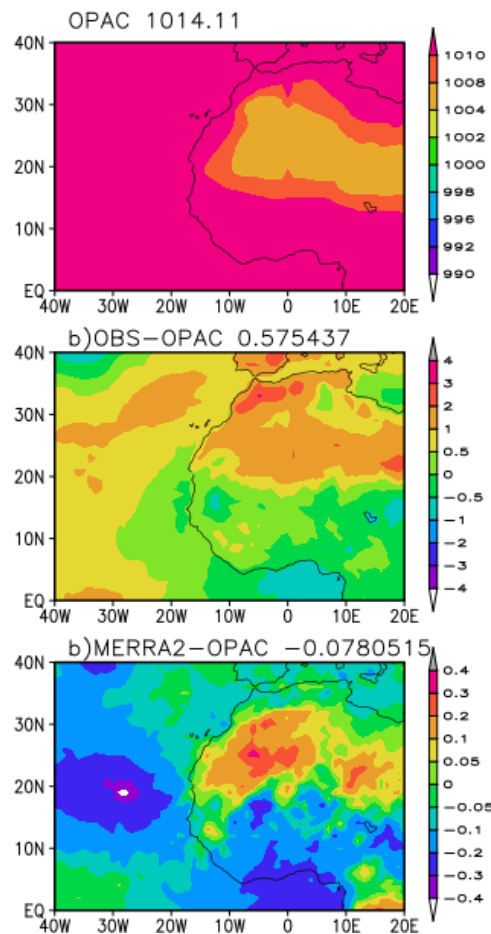


Figure 15. Sea level pressures at T+120 hours averaged for the 2019 summer over Northwest Africa from the OPAC experiment in (a), differences between the NCEP Reanalysis and the OPAC experiment in (b), and differences between the MERRA2 and OPAC experiments in (c).

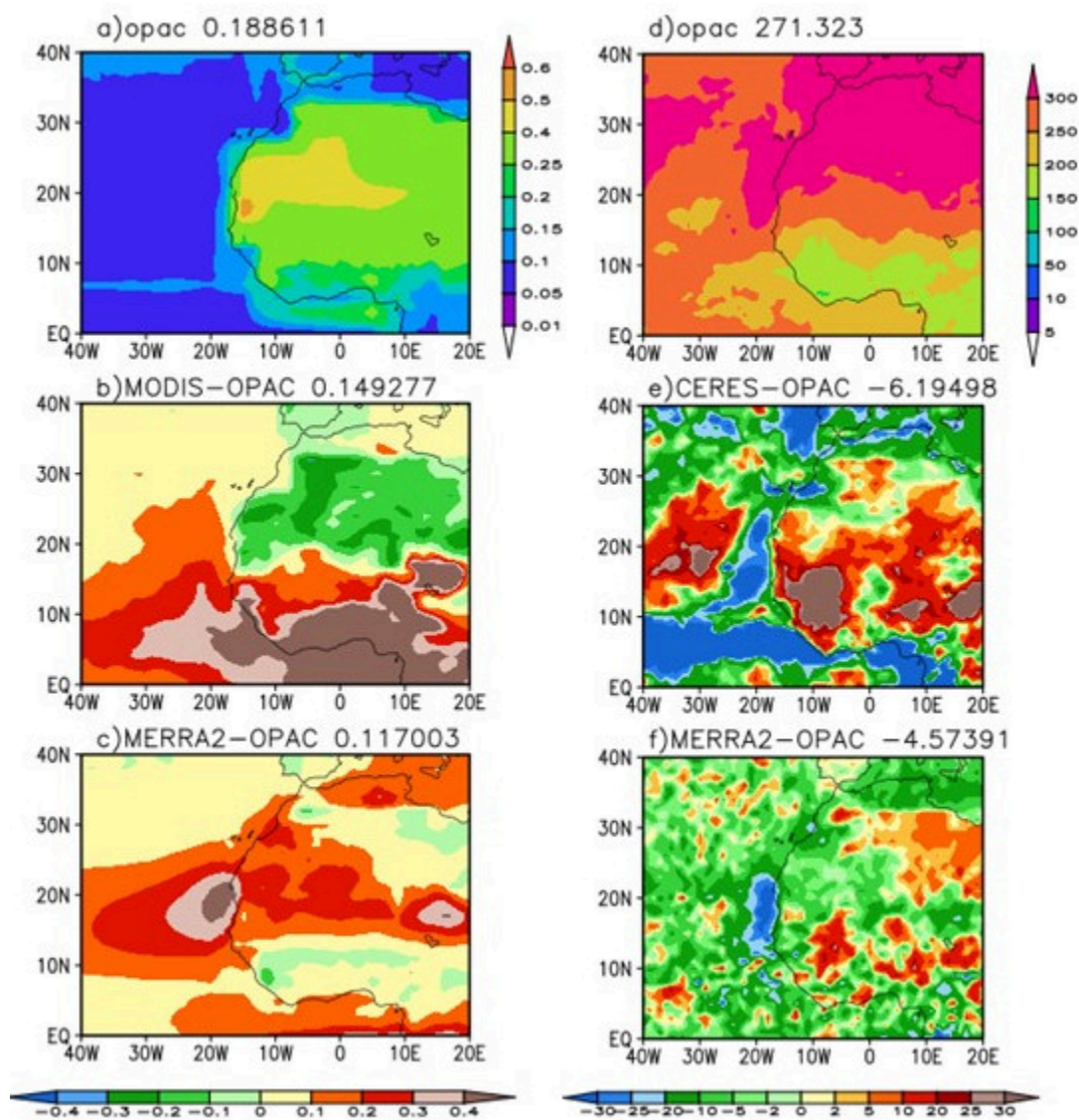


Figure 16. Same as Figure 10 except for the Northwest Africa region.

3.2.3 Impact on East Asian Summer Monsoon Precipitation

The East Asian summer monsoon is primarily driven by the land-sea temperature differences between the Eurasian continent and the Pacific Ocean. The monsoonal flow that carries moist air from the Indian and Pacific Oceans to East Asia shifts northward in the form of quasi-stationary fronts, with a precipitation spike in July and August (e.g., Ding and Chan, 2005). The mean AOD in July from the OPAC experiment shows relatively heavier aerosol loadings over the continent, with three maximum centers located at 38°N and 105°E, at 25°N and 118°E, and over the Korean peninsula (Figure 17a), respectively. However, in comparison with MODIS the OPAC experiment underestimated aerosol loading in most of the continental regions except for the three maximum centers (Figure

17b). The MERRA2 experiment reduced the biases and matched reasonably well with the MODIS observations (Figure 7c).

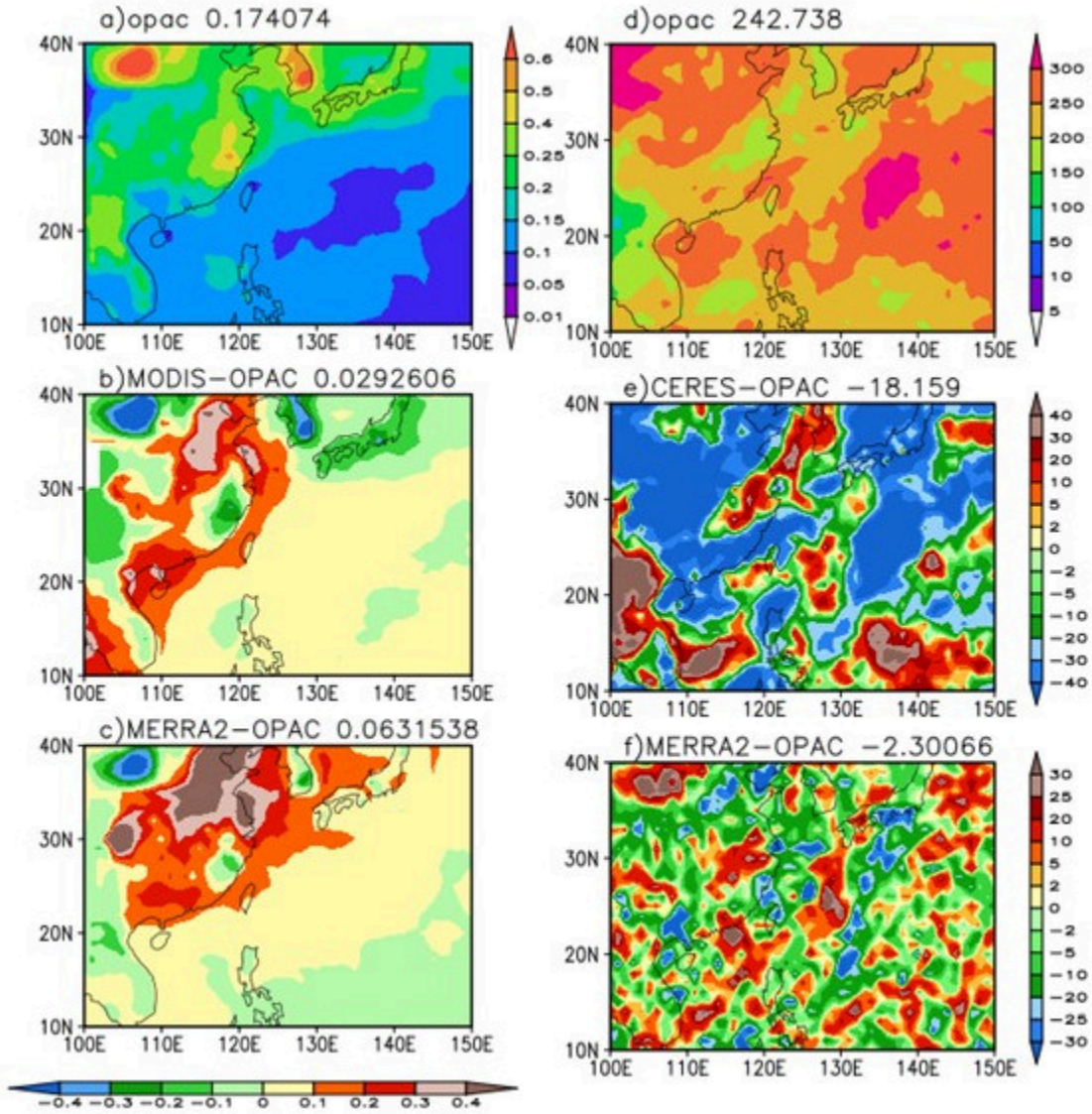


Figure 17. Same as Figure 16 except for Southeast Asia in July.

The surface downward SW fluxes from the OPAC experiment have a low bias compared to CERES observations along the Asian coastlines and over Korea and Japan (Figures 17d and 17e). With a more reasonable representation of aerosols in the MERRA2 experiment, surface downward SW fluxes are improved in the area extending from 12°N and 110°E to 30°N and 130°E, where the AOD is relatively low along and off the Asian coastline.

The MERRA2 experiment also appears to simulate precipitation better than the OPAC experiment in comparison with the NCEP Reanalysis (Figure 18). The increased surface

downward SW and surface heating in the MERRA2 experiment east of the coastline of east Asia might be favorable for upward motion and beneficial for increased precipitation along the coastline for both MERRA2 and observations. The surface cooling from less downward SW from aerosol loading over the East Asian continent might contribute to higher sea-level pressures and less precipitation there (Figure 19) and the heating off the coastline might be related to the lower pressures and enhanced precipitation (Figure 18).

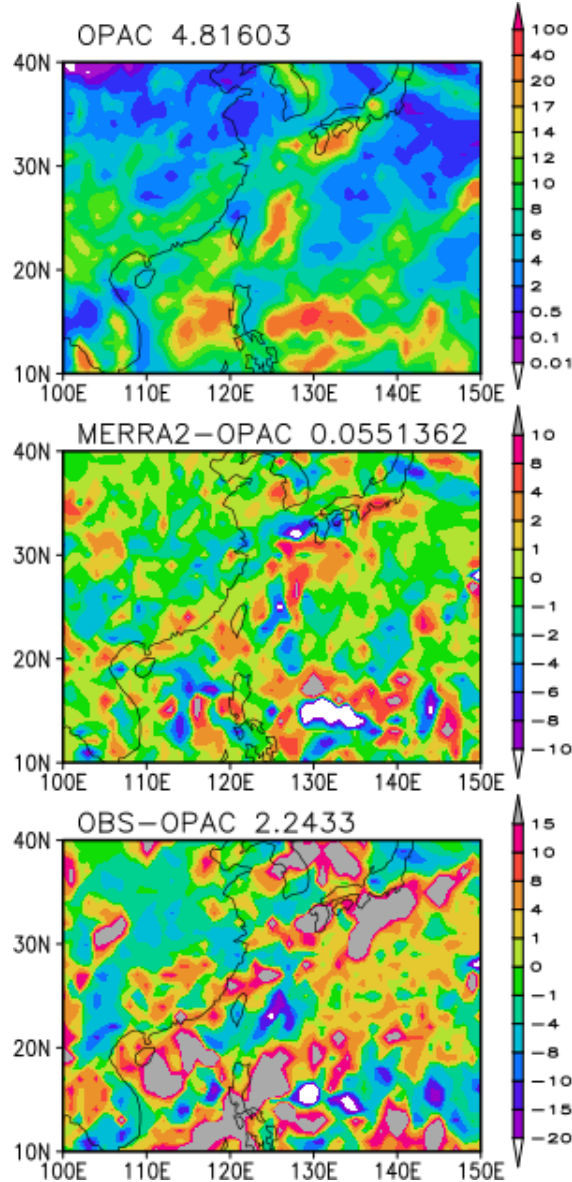


Figure 18. Same as Figure 13 except for Southeast Asia in July.

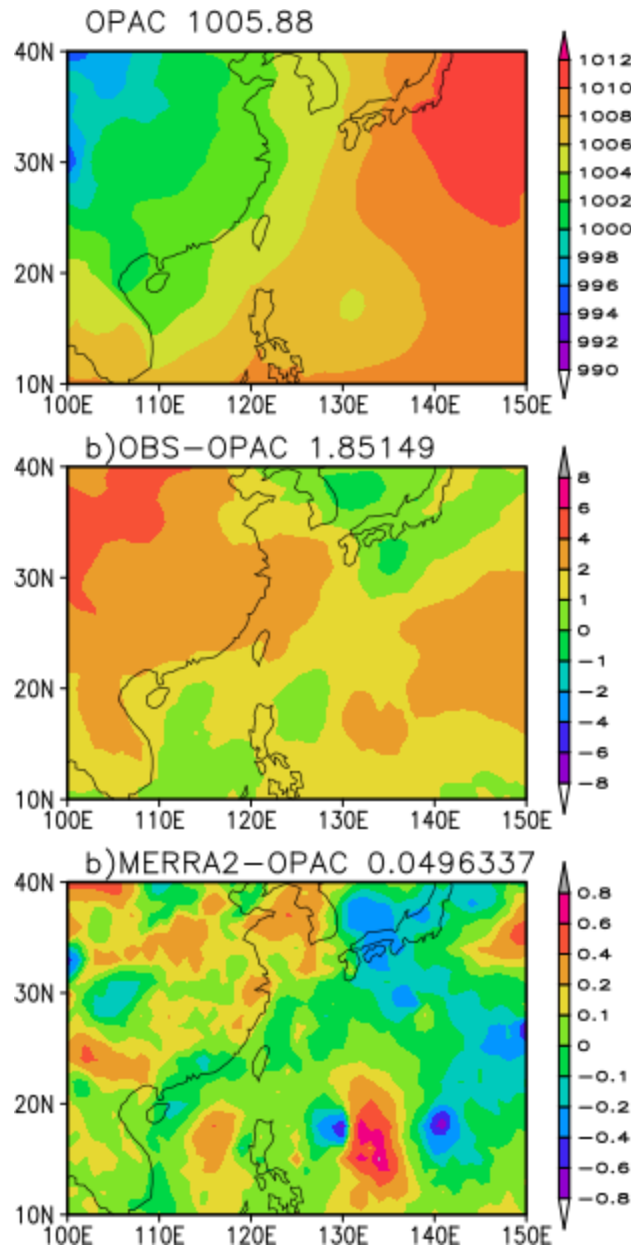


Figure 19. Same as Figure 15 except for Southeast Asia in July.

3.2.4. Impact of Aerosols on Large-Scale NWP Forecast Skill

In this section we examine the impact of aerosol direct radiative forcing on the overall medium-range weather forecast skill. In the previous sections the investigation focused only on the 2019 summer season when the aerosol SW forcing is the largest of the year. For completeness, a winter season is also included in the following evaluation of forecast skill. Shown in Figure 20 are anomaly correlation (AC) scores of 500-hPa height as a function of forecast lead time for the Northern Hemisphere (20°N– 80°N) and Pacific and North America (PNA) region for the 2019 summer and 2019/2020 winter, respectively.

AC score measures how well the synoptic-scale systems over the globe are represented in the model. By using the MERRA2 aerosols, the 500-hPa height AC scores are improved for the Northern Hemisphere and PNA for both the winter and summer seasons. The improvements are statistically significant at the 95% confidence level at certain forecast lead times, such as for the first three days of the Northern Hemisphere summer and for the ninth day of the PNA summer and the Northern Hemisphere winter.

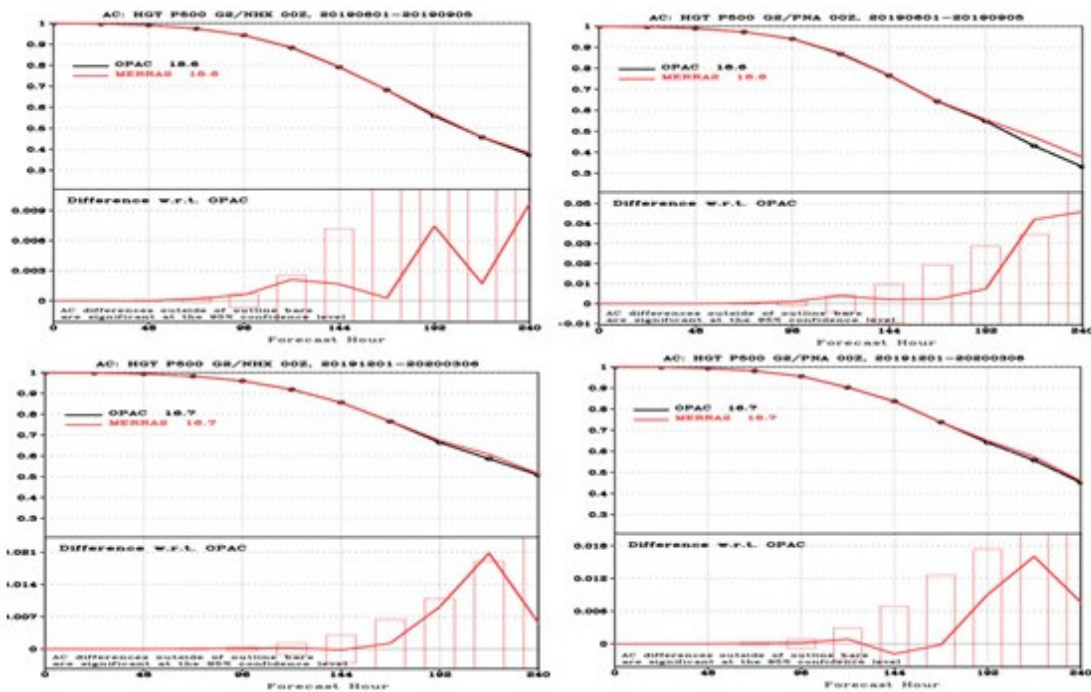


Figure 20. 500-hPa height anomaly correlation scores for the Northern Hemisphere (left panels) and the Pacific North American region (right panels), and for the boreal summer (upper panels) and boreal winter (lower panels), respectively.

4. Discussion and Conclusions

In this study aerosol direct effects on numerical weather forecasting are examined and compared for the OPAC and MERRA2 climatological aerosol datasets. First, four clear-sky cases are chosen for the Sahara Desert, Northeast CONUS, Southern Ocean, and Southeast Asia to perform SCM evaluations. Results show that dust, black carbon, sulfate, and sea salt have similar direct radiative effects on the surface and the atmosphere. Because of the light extinction effect of aerosols, the larger aerosol loading and thus AOD results in a weakened surface downward SW flux. The difference in surface downward SW flux between the SCM runs with the two aerosol datasets reached 30 W/m^2 at certain locations. Aerosols also absorb incoming SW radiation and LW radiation emitted from the surface and the atmosphere, resulting in a warming effect at the layers where aerosol concentrations are high. In turn, this also leads to larger surface downward LW flux. The

change of net radiative flux at the TOA caused by aerosols is largely determined by the reflection of SW radiation at layers where aerosol concentrations are dense. The TOA differences can reach more than 10 W/m^2 .

Then medium-range weather forecast experiments were conducted using the C768L127 GFS for the 2019 summer and 2019/2020 winter seasons to investigate the differences in global AOD between the runs using the OPAC and MERRA2 experiments. Aerosol impacts on atmospheric circulation and precipitation, especially monsoonal rainfall, are investigated. MODIS AOD retrievals, CERES-derived radiative fluxes and the NCEP Reanalysis are used as truth for evaluation. The MERRA2 experiment showed an improvement over the OPAC experiment in the simulation of AOD over the globe in comparison with the MODIS retrievals. The OPAC experiment seriously underestimated AOD over Northwest Africa, central-to-east Africa, Southeast Asia, and the Indo-Gangetic Plain and overestimated AOD in the storm track regions in both the Northern and Southern Hemispheres.

The effects of AOD on the radiation budget found in the global NWP model experiments are generally consistent with those in the SCM runs. The surface downward SW and LW fluxes and TOA SW and OLR are compared against CERES satellite observations. Improvements in radiation fluxes from the MERRA2 experiment were observed in the regions where the OPAC experiment had large AOD biases, such as Northwest Africa and the storm track regions. The patterns are most noticeable for the surface downward SW flux.

The more realistic AOD from the MERRA2 experiment produced more realistic radiative forcing and thus radiative heating/cooling in the atmosphere and at the surface, and improved the simulated circulations and other meteorological fields, especially in regions where aerosol loading is high. In the Indian Monsoon region, aerosol radiative forcing over the Arabian and India peninsulas causes cooling in the lower troposphere and warming in the upper troposphere. Compared to the OPAC experiment, sea-level pressure from the MERRA2 experiment is higher over the continent and lower over the ocean in the monsoon region. The monsoon circulation from the MERRA2 experiments tends to be stronger and compares better with observations. The experiment with MERRA2 in West Africa had a weakening on both the southern and northern flanks of the AEJ, but a strengthening of the jet from a weakened low pressure resulting from reduced aerosol loading, and compared well with NCEP Reanalysis. The experiment with MERRA2 aerosols also has a more realistic AOD representation over the East Asian continent and Pacific Ocean than the experiment with OPAC aerosols. The surface cooling from less downward SW from aerosol loading over the East Asian continent might contribute to the higher sea-level pressures. The increased surface downward SW and surface heating in the MERRA2 experiment east of the Asian coastline might be favorable for upward motion

and beneficial for increased precipitation in both MERRA2 and the observations. As a result, the experiment with MERRA2 aerosols improved the 500-hPa height AC scores in the Northern Hemisphere and PNA region for the winter and summer seasons.

Acknowledgments: The Authors would like to thank Y. Hou, S. Lu, S. Moorthi, R. Pincus, H. Lin, J. Wang, D. Heinzeller, K. Friedman, W. Meng, H. Chuang, Q. Liu, J. Peng, R. Sun, and J. Bao for insightful discussions and their assistance in implementing the MERRA2 aerosols in the UFS model. Mary Hart of EMC is thanked for proofreading the manuscript.

Acronym List:

3DVAR: the three-dimensional variational data analysis
AERONET: Aerosol Robotic Network
AOD: aerosol optical depth
AVHRR: the Advanced Very High Resolution Radiometer
CAMS: Copernicus Atmosphere Monitoring System
CERES: the Earth's Radiant Energy System
DYCOM-II: the Dynamics and Chemistry of Stratocumulus II
ECWMF: European Centre for Medium-Range Weather Forecasts
ERF: The effective radiative forcing
IFS: Integrated Forecasting System
GASS: the Global Atmosphere System Studies
GCSS: the Global Energy and Water Experiment Cloud System Study
GEOS: Geostationary Operational Environmental Satellites
GFDL: Geophysical Fluid Dynamics Laboratory
Gocart: The Goddard Chemistry Aerosol Radiation and Transport
GSI: Gridpoint Statistical Interpolation
LUTs: Looking up tables
NCEP: National Centers for Environmental Prediction
MERRA2: Modern-Era Retrospective analysis for Research and Applications, Version 2
McICA: Monte-Carlo Independent Column Approximation
MISR: Multi Angle Imaging Spectroradiometer
MODIS: Moderate Resolution Imaging Spectroradiometer
OPAC: Optical Properties of Aerosols and Clouds
RRTMG: Rapid Radiation Transfer Model for GCM
SCM: Single Column Model
SCAM5: SCM mode of version 5 of the Community Atmosphere Model

References

Ackerman, A. S., and Coauthors, 2009: Large-eddy simulations of a drizzling, stratocumulus-topped marine boundary layer. *Mon. Wea. Rev.*, **137**, 1083–1110,

doi:10.1175/2008MWR2582.1.

- Boucher, O., D. Randall, P. Artaxo, C. Bretherton, G. Feingold, P. Forster, V.-M. Kerminen, Y. Kondo, H. Liao, U. Lohmann, P. Rasch, S.K. Satheesh, S. Sherwood, B. Stevens and X.Y. Zhang, 2013: Clouds and Aerosols. In: *Climate Change 2013: The Physical Science Basis. Contribution of Working Group I to the Fifth Assessment Report of the Intergovernmental Panel on Climate Change* [Stocker, T.F., D. Qin, G.-K. Plattner, M. Tignor, S.K. Allen, J. Boschung, A. Nauels, Y. Xia, V. Bex and P.M. Midgley (eds.)]. Cambridge University Press, Cambridge, United Kingdom and New York, NY, USA.
- Bozzo, A., S. Remy, A. Benedetti, J. Flemming, P. Bechtold, M.J. Rodwell and J.-J. Morcrette, 2017: Implementation of a CAMS-based aerosol climatology in the IFS. *ECMWF Technical Memoranda*, **801**, 33p.
- Buchard, V., C. A. Randles, A. M. da Silva, A. Darmenov, P. R. Colarco, R. Govindaraju, R. Ferrare, J. Hair, A. J. Beyersdorf, L. D. Ziemba, and H. Yu, 2017: The MERRA-2 Aerosol Reanalysis, 1980-Onward, Part II: Evaluation and Case Studies. *J. Climate*, **30**, 6851–6872.
- Ding, Y. H. and J. C. L. Chan, 2005: The East Asian summer monsoon: an overview. *Meteorol. Atmos. Phys.* **89**, 117–142. DOI 10.1007/s00703-005-0125-z.
- Hess, M., P. Koepke, and I. Schult, 1998: Optical properties of aerosols and clouds: the software package OPAC, *Bulletin of the American Meteorological Society*, **79**, 831–844.
- Hou, Y.-T., S. Moorthi, and K.A. Campana, 2002: Parameterization of solar radiation transfer in the NCEP models. *NCEP Office Note 441*.
- Gautam, R., N.-Y. C. Hsu, S.-C. Tsay, et al., 2011: Accumulation of aerosols over the Indo-Gangetic plains and southern slopes of the Himalayas: distribution, properties and radiative effects during the 2009 pre-monsoon season. *Atmos. Chem. Phys.*, **11** (24): 12841–12863 [10.5194/acp-11-12841-2011].
- Lau, W. K., V. Ramanathan, G. Wu, et al., 2008: The Joint Aerosol–Monsoon Experiment: A New Challenge for Monsoon Climate Research. *Bulletin of the American Meteorological Society*, **89** (3): 369–383 [10.1175/BAMS-89-3-369].
- Lebassi-Habtezion, B. and P. M. Caldwell, 2015: Aerosol specification in single-column Community Atmosphere Model version 5. *Geosci. Model Dev.*, **8**, 817–828
- Lee, D., Y. C. Sud, L. Oreopoulos, et al., 2014: Modeling the influences of aerosols on pre-monsoon circulation and rainfall over Southeast Asia. *Atmos. Chem. Phys.*, **14** (13): 6853–6866 [10.5194/acp-14-6853-2014].
- Leroux M., 2001: *The Meteorology and Climate of Tropical Africa*. Springer. pp. 138–139. ISBN 978-3-540-42636-3.
- Lohmann, U., and J. Feichter, 2005: Global indirect aerosol effects: A review. *Atmos. Chem. Phys.*, **5**, 715–737.
- Mlawer, E.J., S. J. Taubman, P. D. Brown, M. J. Iacono, and S. A. Clough, 1997: Radiative

- transfer for inhomogeneous atmospheres: RRTM, a validated correlated-k model for the longwave. *J. Geophys. Res.*, **102**, 16663–16682.
- Mlawer, E. J., and S. A. Clough, 1998: Shortwave and longwave enhancements in the rapid radiative transfer model. *Proc. Seventh Atmospheric Radiation Measurement (ARM) Science Team Meeting*, San Antonio, TX, U.S. Dept. of Energy, 409–413.
- Mlawer, E.J., M.J. Iacono, R. Pincus, H.W. Barker, L. Oreopoulos and D.L. Mitchell, 2016: Contributions of the ARM Program to Radiative Transfer Modeling for Climate and Weather Applications, The Atmospheric Radiation Measurement Program: The First 20 Years, *Meteor. Monograph*, **57**, Amer. Meteor. Soc.
- Mulcahy, J. P., D. N. Walters, N. Bellouin, and S. F. Milton, 2014: Impacts of increasing the aerosol complexity in the Met Office global numerical weather prediction model. *Atmos. Chem. Phys.*, **14**, 4749-4778, doi:10.5194/acp-14-4749-2014.
- Quaas, J., N. Bellouin, and O. Boucher, 2011: Which of satellite-based or model-based estimates are closer to reality for aerosol indirect forcing? Reply to Penner et al. *Proc. Natl. Acad. Sci. U.S.A.*, **108**, E1099.
- Randles, C. A., A. M. da Silva, V. Buchard, P. R. Colarco, A. Darmenov, R. Govindaraju, Q. Smirnov, B. Holben, R. Ferrare, J. Hair, Y. Shinozuka, and C. J. Flynn, 2017: The MERRA-2 Aerosol Reanalysis, 1980 - Onward, Part I: System Description and Data Assimilation Evaluation. *J. Climate*, **30**, 6823–6850.
- Reale, O., Lau, K. M., and A. D. Silva, 2011: Impact of interactive aerosol on the African Easterly Jet in the NASA GEOS-5 global forecasting system, *Wea. Forecast.*, **26**, 504–519, doi:10.1175/WAFD-10-05025.1.
- Rodwell, M. J. and T. Jung, 2008: Understanding the local and global impacts of model physics changes: an aerosol example, *Q. J. R. Meteorol. Soc.*, **134**, 1479–1497, doi:10.1002/qj.298, 2008.
- Twomey, S., 1977: The influence of pollution on the shortwave albedo of clouds, *J. Atmos. Sci.*, **34**, 1149–1152.
- Yang et al., 2020: Model Upgrade Plan and Initial Results from a Prototype NCEP Global Forecast System Version 16, 10th Conference on Transition of Research to Operations, 100th AMS Annual Meeting, Boston.
<https://ams.confex.com/ams/2020Annual/meetingapp.cgi/Paper/362797>
- Zhou, L., S. Lin, J. Chen, L. Harris, X. Chen, and S. Rees, 2019: Toward Convective-Scale Prediction within the Next Generation Global Prediction System. *Bull. Amer. Meteor. Soc.* doi:10.1175/BAMS-D-17-0246.1.